

## 基于 *N*-乙酰-*L*-半胱氨酸修饰的 $\text{ZnFe}_2\text{O}_4@SiO_2$ 纳米材料手性识别酪氨酸对映异构体

陈少凯 李 新 郭晨晨 魏旖僊 袁赛薇 宋会花\*  
(河北师范大学化学与材料科学学院, 石家庄 050024)

**摘要:** 我们将 *N*-乙酰-*L*-半胱氨酸(NALC)修饰于  $\text{ZnFe}_2\text{O}_4@SiO_2$  纳米材料表面, 制备了一种新型的手性纳米复合物( $\text{ZnFe}_2\text{O}_4@SiO_2$ -NALC), 该材料能够简便、快速及高选择性地识别手性酪氨酸(Tyr)对映体。利用X射线粉末衍射(XRD)、红外光谱(FT-IR)、能量色散X射线光谱(EDS)、扫描电子显微镜(SEM)、高分辨率透射电子显微镜(HRTEM)和振动样品磁力计(VSM)等一系列表征手段对首次合成出的  $\text{ZnFe}_2\text{O}_4@SiO_2$ -NALC 进行测试表征, 并将其应用于对手性识别领域的探究。实验结果表明, 利用光谱技术(紫外-可见光谱和荧光光谱),  $\text{ZnFe}_2\text{O}_4@SiO_2$ -NALC 可对 Tyr 对映异构体进行手性识别。此外, 我们进一步对 Tyr 浓度和 pH 值等实验参数进行了优化。

**关键词:** 手性识别;  $\text{ZnFe}_2\text{O}_4@SiO_2$ -NALC; 手性纳米粒子; 酪氨酸

中图分类号: O611.65 文献标识码: A 文章编号: 1001-4861(2020)11-2169-10

DOI: 10.11862/CJIC.2020.235

### Chiral Discrimination Tyrosine Enantiomers Based on *N*-Acetyl-*L*-cysteine Modified $\text{ZnFe}_2\text{O}_4@SiO_2$ Nanoparticles

CHEN Shao-Kai LI Xin GUO Chen-Chen WEI Yi-Xuan YUAN Sai-Wei SONG Hui-Hua\*  
(College of Chemistry and Material Science, Hebei Normal University, Shijiazhuang 050024, China)

**Abstract:** *N*-acetyl-*L*-cysteine (NALC) functionalized  $\text{ZnFe}_2\text{O}_4@SiO_2$  ( $\text{ZnFe}_2\text{O}_4@SiO_2$ -NALC) was synthesized and exhibited simplicity, rapidity and high selectivity in the separation of chiral tyrosine (Tyr) enantiomers. The chiral nanocomposite of  $\text{ZnFe}_2\text{O}_4@SiO_2$ -NALC was characterized by X-ray powder diffraction (XRD), infrared spectroscopy (FT-IR), energy dispersive X-ray spectroscopy (EDS), scanning electron microscopy (SEM), high resolution transmission electron microscopy (HRTEM) and vibrating sample magnetometer (VSM). This is the first synthesis of  $\text{ZnFe}_2\text{O}_4@SiO_2$ -NALC for chiral recognition. The proposed optical spectroscopic techniques (UV-Vis spectrum and fluorescence spectra) showed excellent enantiospecificity for Tyr enantiomers. Furthermore, the experimental parameters such as the Tyr concentration and the pH values were optimized.

**Keywords:** chiral recognition;  $\text{ZnFe}_2\text{O}_4@SiO_2$ -NALC; chiral nanoparticles; tyrosine

## 0 Introduction

Chirality is ubiquitous in our real life, and it is the basic feature of our life processes. Most biological elements, medical drugs and many organic molecules are

chiral molecules<sup>[1]</sup>. Due to the particular characteristics of chiral substances in physiological activities and life processes, the application and development of chiral substances in pharmaceuticals, biochemistry, asymmetric catalysts make more and more research groups

收稿日期: 2020-03-28。收修改稿日期: 2020-08-28。

河北省自然科学基金(No.B2018205152)和河北省引进留学人员基金(No.CL201715)资助项目。

\*通信联系人。E-mail: songhuihua@mail.hebtu.edu.cn, Tel: +86-0311-80787400

begin to study the phenomenon of chirality.

Since a pair of enantiomers can exhibit different chemical properties, physiological and pharmacological activities under the same environment, so the identification of enantiomers is very important in the chiral field<sup>[2]</sup>. At the same time, chiral recognition is one of the important and special modes of molecular recognition, which has aroused widespread concern<sup>[3]</sup>. Currently, there are many methods for chiral analyses, such as chiral ligand exchange chromatography (CLEC), high performance liquid chromatography (HPLC), gas chromatography (GC), capillary electrophoresis (CE)<sup>[4]</sup>. However, these existing analytical tests strongly rely on expensive chiral columns and their operation is complicated, so it is necessary to find a method for distinguishing chiral enantiomers with low cost, less time-consuming and simple operation. Recently, recognition of chiral molecules has been developed based on optical spectroscopic techniques (such as fluorescence and ultraviolet-visible), electrochemistry, and circular dichroism (CD). These techniques have drawn special attention for discrimination of two enantiomers<sup>[5]</sup>.

Due to the unique properties of metal nanoparticles with grain boundary ratio, surface energy ratio and surface atomic ratio, more and more research teams have used metal nanoparticles for chiral recognition<sup>[2-4]</sup>. Most of the nanomaterials used for chiral recognition are chiral precious metal nanomaterials<sup>[5-11]</sup> and quantum dots<sup>[12-16]</sup>. However, these nanomaterials require harsh preparation conditions or relatively high synthesis costs, so it's necessary to prepare a simple and inexpensive nanomaterial for chiral recognition. Magnetic nanomaterials are cheap, easy to obtain, and have great potential in high-efficiency separation, sensitive measurement and selective catalysis. After using a chiral selector to modify the magnetic nanoparticles, the prepared composite material not only has its own magnetic properties but also has chirality<sup>[17]</sup>. Therefore, magnetic nanomaterials modified by chiral ligands have great potential in chiral recognition. Among the spinel-structured magnetic oxides,  $\text{ZnFe}_2\text{O}_4$  is a relatively special type of magnetic oxide because of its simple synthesis process, short synthesis cycle and low prepara-

tion cost. It is widely used in various fields of research<sup>[18]</sup>, but application of chiral identification is still scarce. In this work, we choose  $\text{ZnFe}_2\text{O}_4$  as a core material to explore its recognition ability. Due to the obvious aggregation phenomenon between magnetic nanoparticles, we need to find a solution that can reduce this phenomenon. Changing the particle morphology is an effective method. For example, the use of inorganic compounds to coat magnetic nanoparticles can alleviate the aggregation phenomenon caused by magnetism. As the first choice of shell material,  $\text{SiO}_2$  can not only reduce the interaction between magnetic particles but also play a certain stabilizing effect<sup>[19]</sup>. *N*-acetyl-*L*-cysteine (NALC) was chosen as a chiral candidate for modifying the nanoparticles due to its chiral structure, and it can be bound to the surface of nanoparticles via the -SH and -COOH bonds through heating reflux.

Our laboratory has reported that NALC, as a chiral modifier, was loaded on  $\text{CuFe}_2\text{O}_4@ \text{SiO}_2$  nanoparticles surface, and the product was taken as chiral probes for recognition of chiral tyrosine enantiomers by using UV-Vis spectrum<sup>[20]</sup>. To further explore the mechanism of chiral recognition, NALC-capped  $\text{ZnFe}_2\text{O}_4@ \text{SiO}_2$  ( $\text{ZnFe}_2\text{O}_4@ \text{SiO}_2$ -NALC) was synthesized and characterized by X-ray powder diffraction (XRD), infrared spectroscopy (FT-IR), energy dispersive X-ray spectroscopy (EDS), scanning electron microscopy (SEM), high resolution transmission electron microscopy (HRTEM) and vibrating sample magnetometer (VSM). The results showed that the nanomaterial can recognize the *L*-/*D*-Tyr through ultraviolet-visible spectroscopy and fluorescence spectroscopy.

## 1 Experimental

### 1.1 Reagents

$\text{ZnCl}_2$ , sodium hydroxide and absolute ethanol were purchased from Tianjin Yongda Chemical Reagent Co., Ltd (Tianjin, China).  $\text{FeCl}_3 \cdot 6\text{H}_2\text{O}$  was purchased from Shanghai Maclean Biochemical Technology Co., Ltd (Shanghai, China). NALC, tetraethyl orthosilicate (TEOS) and *L*-/*D*-Tyr were purchased from Beijing Belling Way Reagent Company (Beijing,

China). Ammonium hydroxide was purchased from Tianjin Kaitong Chemical Reagent Company Limited (Tianjin, China).

## 1.2 Instrumentation

The UV-Vis spectrum was recorded on a U-3010 Spectrophotometer (Hitachi, Japan) at room temperature. The fluorescence spectra was acquired by a Fluorescence Spectrometer (FS5) (Edinburgh Instruments, United Kingdom). The FT-IR spectra was acquired on a FT-IR-8900 spectrometer system from 4 000 to 400  $\text{cm}^{-1}$  (KBr pellets) (Shimadzu Corporation, Japan). The powder XRD patterns were collected on a Bruker D8-Advance X-ray diffractometer using  $\text{Cu K}\alpha$  radiation ( $\lambda = 0.154\ 2\ \text{nm}$ ,  $U=40\ \text{kV}$ ,  $I=40\ \text{mA}$ ) in  $2\theta$  range of  $10^\circ \sim 80^\circ$  at room temperature. The SEM and EDS were taken with a S-4800 Cold Field Emission Scanning Electron Microscope at an acceleration voltage of 3 kV (Hitachi, Japan). The HRTEM was conducted on Hitachi H-7650 (Hitachi, Japan). VSM were tested by 735 Vibrating sample magnetometer (LAKESHORE, USA).

## 1.3 Preparation of $\text{ZnFe}_2\text{O}_4$ nanoparticles

$\text{ZnFe}_2\text{O}_4$  nanoparticles (NPs) were synthesized by the chemical co-precipitation method.  $\text{FeCl}_3 \cdot 6\text{H}_2\text{O}$  (10 mmol) and  $\text{ZnCl}_2$  (5 mmol) were dissolved in deionized water (100 mL), and stirred vigorously using magnetic stirrer for 2 h at room temperature. Then the pH value of the solution was adjusted to about 13 by addition of a dilute aqueous NaOH solution, then the mixture was stirred magnetically for 6 h. The resulting precipitate was filtered, washed with deionized water and absolute ethanol until the pH value reached 7, and calcined at 500  $^\circ\text{C}$  to obtain  $\text{ZnFe}_2\text{O}_4$  nanoparticles.

## 1.4 Preparation of $\text{ZnFe}_2\text{O}_4@/\text{SiO}_2$ core-shell nanoparticles

$\text{ZnFe}_2\text{O}_4$  (1 g) was added to a mixed solution of distilled water (20 mL) and absolute ethanol (60 mL), and the solution was sonicated for 15 min to achieve the dispersion. The concentrated ammonia water (2 mL) was added to the above solution immediately, then tetraethyl orthosilicate (TEOS, 0.5 mL) was added dropwise to the above solution slowly under stirring vigorously. The resulting solution was mechanically stirred for 12 h at room temperature, and the products were

collected by centrifuged, washed three times with deionized water and absolute ethanol respectively, and dried at 60  $^\circ\text{C}$  for 3 h.

## 1.5 Surface modification of $\text{ZnFe}_2\text{O}_4@/\text{SiO}_2$ with NALC

$\text{ZnFe}_2\text{O}_4@/\text{SiO}_2$  (1 g) was dispersed in absolute ethanol (10 mL) using an ultrasonic bath for 30 min. Then, NALC (0.6 g) and  $\text{H}_2\text{SO}_4$  (1 mL, 98%) were added to the above solution. This solution was heated under reflux conditions, and the color changes from reddish brown to light yellow green. After completion of the reflux heating, the solution was mechanically stirred overnight to allow for the completion of the reaction. The resulting nanoparticles were separated using centrifugation, washed with absolute ethanol, and dried at 60  $^\circ\text{C}$  for 3 h to get  $\text{ZnFe}_2\text{O}_4@/\text{SiO}_2$ -NALC chiral core-shell nanomaterial.

## 2 Results and discussion

### 2.1 Characterization of the nanoparticles

#### 2.1.1 FT-IR analysis

The FT-IR spectra of  $\text{ZnFe}_2\text{O}_4$ ,  $\text{ZnFe}_2\text{O}_4@/\text{SiO}_2$ ,  $\text{ZnFe}_2\text{O}_4@/\text{SiO}_2$ -NALC and NALC are shown in Fig. 1. In the infrared spectrum of  $\text{ZnFe}_2\text{O}_4$  (Fig. 1a), a strong and sharp absorption band appeared at  $\sim 570\ \text{cm}^{-1}$  is the O-M characteristic vibration absorption peak<sup>[21-22]</sup>, which is the characteristic absorption peak of zinc ferrite. New peaks at 1 092, 796 and 468  $\text{cm}^{-1}$  were observed for  $\text{ZnFe}_2\text{O}_4@/\text{SiO}_2$  and  $\text{ZnFe}_2\text{O}_4@/\text{SiO}_2$ -NALC (Fig. 1b and 1c), which equivalent of the typical sym-

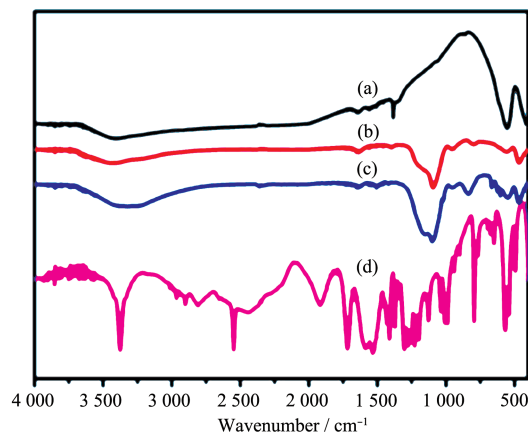


Fig.1 FT-IR spectra of (a)  $\text{ZnFe}_2\text{O}_4$ , (b)  $\text{ZnFe}_2\text{O}_4@/\text{SiO}_2$ , (c)  $\text{ZnFe}_2\text{O}_4@/\text{SiO}_2$ -NALC and (d) NALC

metric and bending vibrations of Si-O-Si<sup>[23-27]</sup>. These results prove that the SiO<sub>2</sub> shell has been successfully loaded on the material surface.

The FT-IR spectrum of NALC exhibited a series of typical characteristic peaks of amino acids. It is worth noting that, a weak band near 2 550 cm<sup>-1</sup> virtually confirms the presence of -SH group in NALC molecule. When NALC bound on the surface of ZnFe<sub>2</sub>O<sub>4</sub>@SiO<sub>2</sub> (Fig. 1c), a dramatic collapse occurred in a range of 1 150~1 300 cm<sup>-1</sup><sup>[28]</sup>, and the peaks at 1 018 and 1 103 cm<sup>-1</sup> are related to the stretching of C-O and C-N bonds<sup>[29]</sup>, so it can be proved that there is NALC in the sample. Concurrently, the -SH stretching band at 2 550 cm<sup>-1</sup> of NALC disappeared in the IR spectrum of NALC-modified ZnFe<sub>2</sub>O<sub>4</sub>@SiO<sub>2</sub> nanoparticles, which indicates that the NALC and the nanoparticles are bonded by the -SH bond. In addition, the decrease of stretching vibration peak of -COOH at 1 720 cm<sup>-1</sup> indicates that the carboxylic acid structure in NALC molecule is deprotonated<sup>[30]</sup>. This deprotonation process is assisted by the interaction of the carboxylic acid group with the ZnFe<sub>2</sub>O<sub>4</sub>@SiO<sub>2</sub> surface, which acts as a proton acceptor<sup>[31]</sup>. Therefore, the IR spectrum show that ZnFe<sub>2</sub>O<sub>4</sub>@SiO<sub>2</sub> is compatible with NALC through the binding of the two groups (-SH and -COOH)<sup>[31]</sup>. The structure of ZnFe<sub>2</sub>O<sub>4</sub>@SiO<sub>2</sub>-NALC is shown in Fig.2.

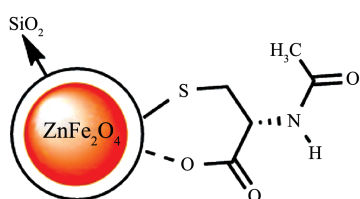


Fig.2 Structure of ZnFe<sub>2</sub>O<sub>4</sub>@SiO<sub>2</sub>-NALC

### 2.1.2 XRD analysis

The XRD patterns of ZnFe<sub>2</sub>O<sub>4</sub>, ZnFe<sub>2</sub>O<sub>4</sub>@SiO<sub>2</sub>, and ZnFe<sub>2</sub>O<sub>4</sub>@SiO<sub>2</sub>-NALC are shown in Fig.3. The powder XRD patterns of ZnFe<sub>2</sub>O<sub>4</sub> could be assigned to ZnFe<sub>2</sub>O<sub>4</sub> with a cubic spinel structure (PDF No.01-082-1049). The XRD diffraction peaks of ZnFe<sub>2</sub>O<sub>4</sub>@SiO<sub>2</sub> are similar to the ZnFe<sub>2</sub>O<sub>4</sub>, indicating that the SiO<sub>2</sub> shell coated on the surface of ZnFe<sub>2</sub>O<sub>4</sub> is amorphous<sup>[32-33]</sup>. We also used the purchased pure NALC for XRD test. The test result is shown in Fig.3, and we

could see that the synthesized ZnFe<sub>2</sub>O<sub>4</sub>@SiO<sub>2</sub>-NALC nanomaterial exhibits characteristic peaks of NALC at 2 $\theta$ =18.34°, 26.08° and 28.74°. Therefore, the ZnFe<sub>2</sub>O<sub>4</sub>@SiO<sub>2</sub>-NALC chiral nanomaterial was successfully synthesized. ZnFe<sub>2</sub>O<sub>4</sub>@SiO<sub>2</sub>-NALC peaks showed some irregular shift or broadening, which may be attributed to the amorphous nature of the NALC structure and its influence on the crystal morphology<sup>[5,34]</sup>.

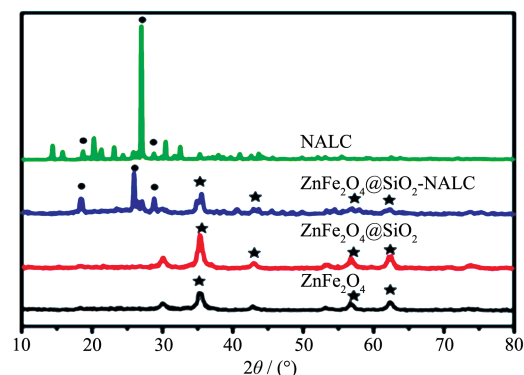


Fig.3 XRD patterns of (a) ZnFe<sub>2</sub>O<sub>4</sub>, (b) ZnFe<sub>2</sub>O<sub>4</sub>@SiO<sub>2</sub> and (c) ZnFe<sub>2</sub>O<sub>4</sub>@SiO<sub>2</sub>-NALC

### 2.1.3 VSM analysis

The magnetization curves of ZnFe<sub>2</sub>O<sub>4</sub>, ZnFe<sub>2</sub>O<sub>4</sub>@SiO<sub>2</sub> and ZnFe<sub>2</sub>O<sub>4</sub>@SiO<sub>2</sub>-NALC measured at 300 K are shown in Fig. 4. The magnetization curve was approximately a straight line, which proves all materials are paramagnetic<sup>[21]</sup>. After the ZnFe<sub>2</sub>O<sub>4</sub> nanoparticles were coated or modified by SiO<sub>2</sub> and NALC, the paramagnetic decreased, which further proves that the synthesis of chiral nanomaterials is successful.

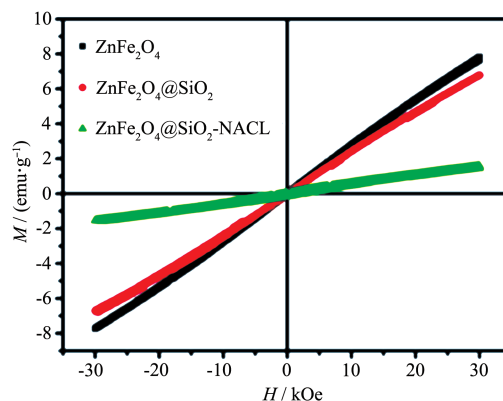


Fig.4 Magnetization curves for ZnFe<sub>2</sub>O<sub>4</sub>, ZnFe<sub>2</sub>O<sub>4</sub>@SiO<sub>2</sub> and ZnFe<sub>2</sub>O<sub>4</sub>@SiO<sub>2</sub>-NALC measured at 300 K

### 2.1.4 EDS analysis

According to the EDS spectrum (Fig.5a), the prod-

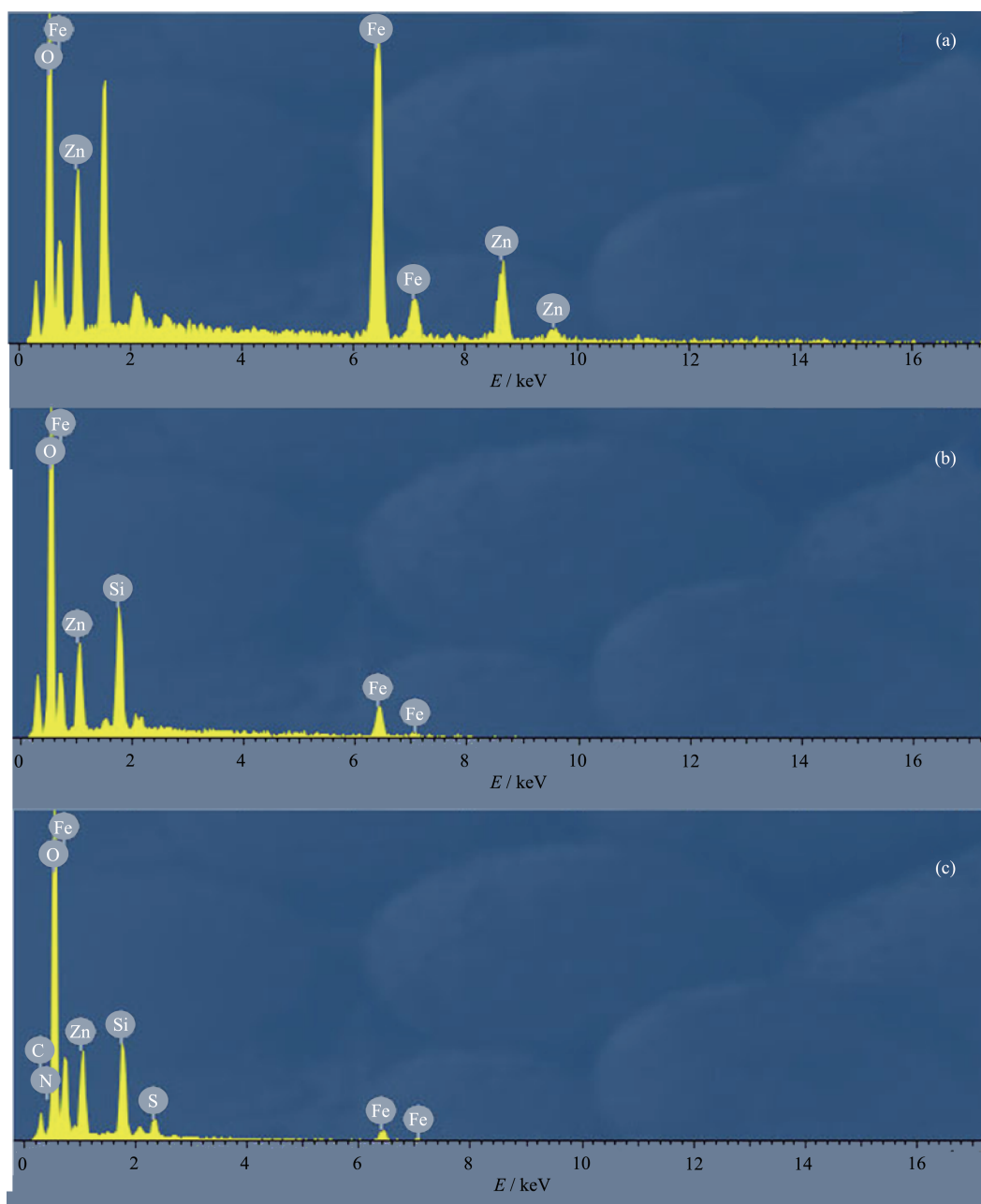


Fig.5 EDS spectra of (a)  $\text{ZnFe}_2\text{O}_4$ , (b)  $\text{ZnFe}_2\text{O}_4@/\text{SiO}_2$  and (c)  $\text{ZnFe}_2\text{O}_4@/\text{SiO}_2\text{-NALC}$

uct is composed of Zn, O, Fe elements, which can prove that the product is  $\text{ZnFe}_2\text{O}_4$ . As shown in Fig.5b, there were Zn, O, Fe, Si elements, which can be attributed to  $\text{ZnFe}_2\text{O}_4@/\text{SiO}_2$ . Fig.5c is EDS spectrum of  $\text{ZnFe}_2\text{O}_4@/\text{SiO}_2\text{-NALC}$ , the compound contained C, N, Fe, Zn, O, Si, S elements, which proves that it is  $\text{ZnFe}_2\text{O}_4@/\text{SiO}_2\text{-NALC}$  chiral compound.

#### 2.1.5 SEM and HRTEM analysis

The specific morphology and structural features of pure  $\text{ZnFe}_2\text{O}_4$ ,  $\text{ZnFe}_2\text{O}_4@/\text{SiO}_2$ , and  $\text{ZnFe}_2\text{O}_4@/\text{SiO}_2\text{-}$

NALC were characterized by SEM (Fig.6) and HRTEM (Fig.7). The average diameter of bare  $\text{ZnFe}_2\text{O}_4$  particles was about 7 nm, and the aggregation phenomenon was obvious. After  $\text{ZnFe}_2\text{O}_4$  was coated with  $\text{SiO}_2$ , SEM and HRTEM images show that  $\text{SiO}_2$  covered multiple aggregated  $\text{ZnFe}_2\text{O}_4$  nanoparticles to form a core-shell structure with a thickness of about 30 nm (Fig.6b and 7b). Fig.6c and 7c show the SEM and HRTEM images of  $\text{ZnFe}_2\text{O}_4@/\text{SiO}_2$  surface modification with NALC. The morphology is similar to that of previously synthesized

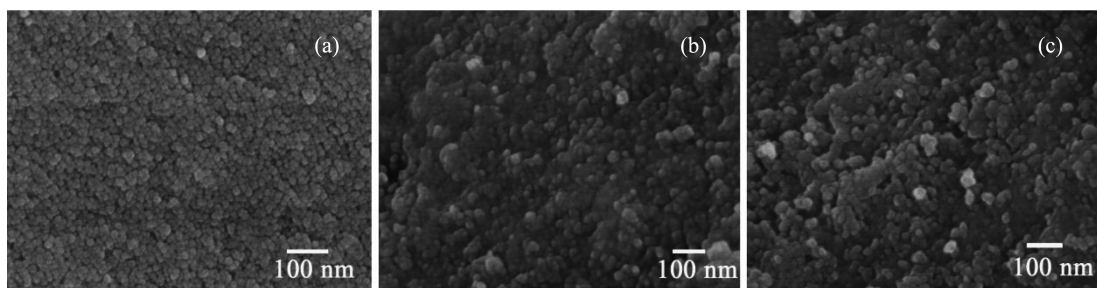


Fig.6 SEM images of (a) ZnFe<sub>2</sub>O<sub>4</sub>, (b) ZnFe<sub>2</sub>O<sub>4</sub>@SiO<sub>2</sub> and (c) ZnFe<sub>2</sub>O<sub>4</sub>@SiO<sub>2</sub>-NALC

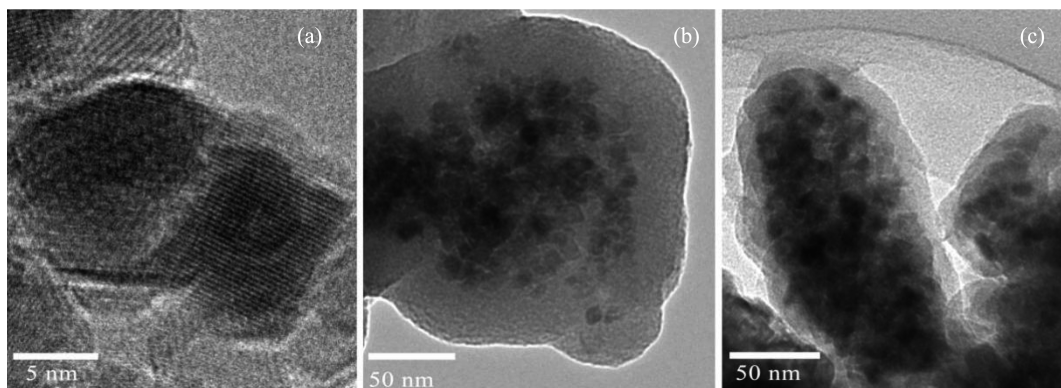


Fig.7 HRTEM images of (a) ZnFe<sub>2</sub>O<sub>4</sub>, (b) ZnFe<sub>2</sub>O<sub>4</sub>@SiO<sub>2</sub> and (c) ZnFe<sub>2</sub>O<sub>4</sub>@SiO<sub>2</sub>-NALC

ZnFe<sub>2</sub>O<sub>4</sub>@SiO<sub>2</sub>.

## 2.2 Enantioselective recognition of Tyr enantiomers

### 2.2.1 Procedures for chiral recognition to *L*-/*D*-Tyr by UV-Vis spectrum

The enantioselective interaction of ZnFe<sub>2</sub>O<sub>4</sub>@SiO<sub>2</sub>-NALC chiral nanomaterials can be probed using UV-Vis spectrum.

As shown in Fig.S1 (Supporting information), tyrosine has absorption peaks at wavelengths of 220 and 274 nm, respectively. The UV absorption of *L*-/*D*-Tyr is completely coincident when the concentration of Tyr is the same. The same conclusion could be obtained with different concentrations of *L*-/*D*-Tyr, as shown in Fig. S1b and S1c. Fig.S1d presents the UV-Vis spectrum of ZnFe<sub>2</sub>O<sub>4</sub>@SiO<sub>2</sub> and ZnFe<sub>2</sub>O<sub>4</sub>@SiO<sub>2</sub>-NALC nanoparticles, it can be concluded that the nanomaterials have no obvious absorption peak at 200 to 500 nm.

In order to study the chiral recognition ability of ZnFe<sub>2</sub>O<sub>4</sub>@SiO<sub>2</sub>-NALC, the nanoparticles were added into *L*-Tyr or *D*-Tyr solution, respectively. As shown in Fig.8, the absorbance of *L*-/*D*-Tyr changed significantly after adding chiral nanomaterial. The *D*-Tyr solution

showed significantly lower absorbance than *L*-Tyr solution.

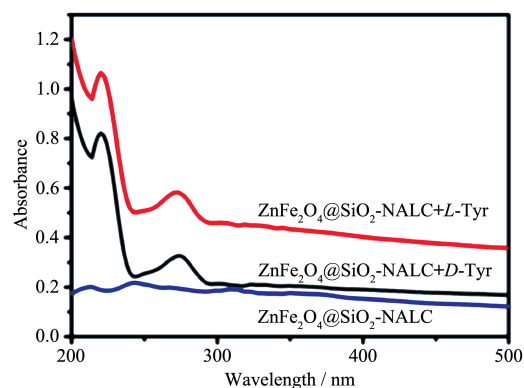


Fig.8 UV-Vis spectra of ZnFe<sub>2</sub>O<sub>4</sub>@SiO<sub>2</sub>-NALC to *D*- or *L*-Tyr (0.075 mmol·L<sup>-1</sup>)

In order to verify the universality of the experimental results, same experimental operation was carried out with different concentrations of Tyr. In the presence of ZnFe<sub>2</sub>O<sub>4</sub>@SiO<sub>2</sub>-NALC, the absorbance of *L*-Tyr or *D*-Tyr with different concentrations is shown in Fig. 9. Absorbance changes in the assay mixtures recorded at 220 and 274 nm are shown in Fig.10 and Table 1 and 2. These results show that the absorbance of *D*-Tyr solution is significantly lower than that of *L*-

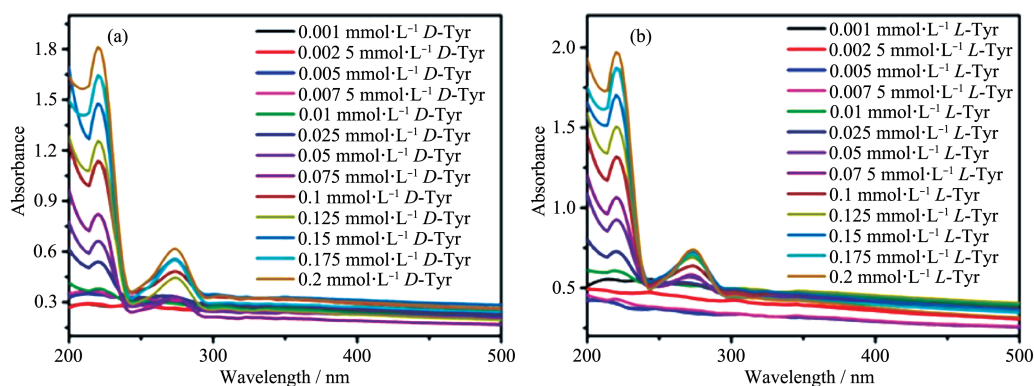


Fig.9 UV-Vis absorption spectra of  $\text{ZnFe}_2\text{O}_4@/\text{SiO}_2$ -NALC in the presence of (a) *D*-Tyr or (b) *L*-Tyr with different concentrations

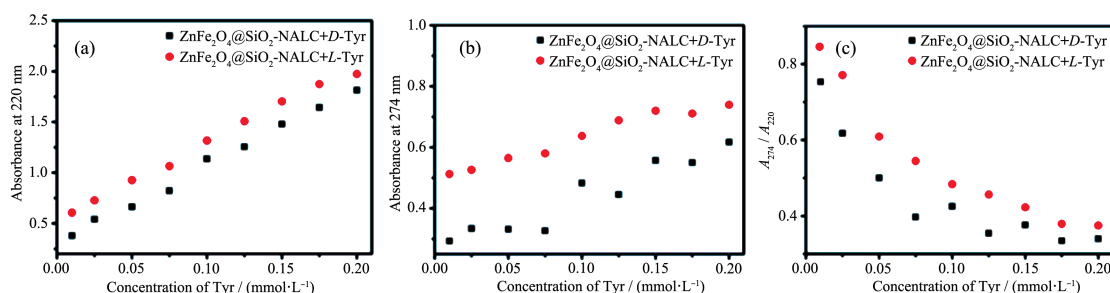


Fig.10 (a) Relationship between absorbance and Tyr concentration at 220 nm; (b) Relationship between absorbance and Tyr concentration at 274 nm; (c) Plot of absorbance ratio  $A_{274}/A_{220}$  and *D*- or *L*-Tyr concentration over a range of 0.01~0.25  $\text{mmol}\cdot\text{L}^{-1}$

**Table 1** Absorbance at 220 nm of  $\text{ZnFe}_2\text{O}_4@/\text{SiO}_2$ -NALC in the presence of *D*-Tyr or *L*-Tyr with different concentrations

$c_{\text{Tyr}} /$ ( $\text{mmol}\cdot\text{L}^{-1}$ )	Absorbance of $\text{ZnFe}_2\text{O}_4@/\text{SiO}_2$ -NALC at 220 nm	
	<i>L</i> -Tyr	<i>D</i> -Tyr
0.010	0.379	0.606
0.025	0.540	0.727
0.050	0.663	0.926
0.075	0.822	1.064
0.100	1.136	1.317
0.125	1.255	1.507
0.150	1.479	1.703
0.175	1.644	1.873
0.200	1.814	1.973

**Table 2** Absorbance at 274 nm of  $\text{ZnFe}_2\text{O}_4@/\text{SiO}_2$ -NALC in the presence of *D*-Tyr or *L*-Tyr with different concentrations

$c_{\text{Tyr}} /$ ( $\text{mmol}\cdot\text{L}^{-1}$ )	Absorbance of $\text{ZnFe}_2\text{O}_4@/\text{SiO}_2$ -NALC at 274 nm	
	<i>L</i> -Tyr	<i>D</i> -Tyr
0.010	0.292	0.512
0.025	0.333	0.526
0.050	0.331	0.564
0.075	0.326	0.580
0.100	0.483	0.637
0.125	0.445	0.688
0.150	0.557	0.720
0.175	0.549	0.710
0.200	0.617	0.739

Tyr solution in the presence of  $\text{ZnFe}_2\text{O}_4@/\text{SiO}_2$ -NALC with the same concentration. The experiment result indicates that  $\text{ZnFe}_2\text{O}_4@/\text{SiO}_2$ -NALC chiral nanoparticles can be used as a probe to detect chiral Tyr enantiomer<sup>[32]</sup>. As shown in Fig. 10c and Table 3, a dramatic experimental phenomenon in the absorbance ratio ( $A_{274}/A_{220}$ ) of  $\text{ZnFe}_2\text{O}_4@/\text{SiO}_2$ -NALC was observed. Obviously, there is a difference in the absorbance ratio ( $A_{274}/A_{220}$ )

between the two enantiomers in each case, and the absorbance ratio of *D*-Tyr ( $A_{274}/A_{220}$ ) is always lower than that of *L*-Tyr at the same amino acid concentration<sup>[10,35]</sup>. These experimental results show that chiral  $\text{ZnFe}_2\text{O}_4@/\text{SiO}_2$ -NALC nanoparticles can identify tyrosine by ultraviolet-visible spectroscopy in solution. There was a good linear relationship between the maximum absorbance at 220 nm in the UV-Vis spectrum and the con-

**Table 3** Absorbance ratio  $A_{274}/A_{220}$  of  $\text{ZnFe}_2\text{O}_4@\text{SiO}_2$ -NALC in the presence of *D*-Tyr or *L*-Tyr with different concentrations

$c_{\text{Tyr}} /$ ( $\text{mmol} \cdot \text{L}^{-1}$ )	$A_{274}/A_{220}$ of $\text{ZnFe}_2\text{O}_4@\text{SiO}_2$ -NALC	
	<i>L</i> -Tyr	<i>D</i> -Tyr
0.010	1.028	0.754
0.025	1.224	1.069
0.050	1.152	1.015
0.075	1.258	1.106
0.100	1.103	1.157
0.125	1.145	1.136
0.150	1.188	1.375
0.175	1.260	1.191
0.200	1.419	1.305

centration of tyrosine enantiomer (0.010~0.250  $\text{mmol} \cdot \text{L}^{-1}$ ), and the lowest detection limit of tyrosine is 10  $\mu\text{mol} \cdot \text{L}^{-1}$ .

The pH value of the solution is a critical parameter of chiral recognition. Here, using Britton-Robinson (B-R) buffer and phosphate buffer to adjust the pH value of the solution, we explored the ability of  $\text{ZnFe}_2\text{O}_4@\text{SiO}_2$ -NALC nanoparticles to recognize tyrosine in a pH range of 2.36~9.18. The experimental results are shown in Fig. S2~S4 and Table S1~S15. The results showed that when the solution was acidic or alkaline, the absorbance of *D*-Tyr system might be higher, lower or the same as that of *L*-Tyr with the increase of tyrosine concentration. The above results show that  $\text{ZnFe}_2\text{O}_4@\text{SiO}_2$ -NALC nanoparticles can only recognize Tyr enantiomer in neutral environment.

### 2.2.2 Procedures for chiral recognition *L*-/*D*-Tyr by

### fluorescence spectra

As the second proof that nanomaterials recognize tyrosine, the fluorescence properties of different concentrations of tyrosine were investigated as shown in Fig. S5. It is obvious that *L*-Tyr exhibited similar fluorescence absorbance to *D*-Tyr when no substance was added and a peak emerged at 304 nm ( $\lambda_{\text{ex}}=229$  nm) in the fluorescence emission spectra.

As shown in Fig. 11, when the concentration of Tyr was 0.175  $\text{mmol} \cdot \text{L}^{-1}$ , the fluorescence intensity of  $\text{ZnFe}_2\text{O}_4@\text{SiO}_2$ -NALC system with *L*-Tyr was significantly higher than that of  $\text{ZnFe}_2\text{O}_4@\text{SiO}_2$ -NALC system with *D*-Tyr. In order to investigate whether the results are universal, we also explored the influence of different Tyr concentrations on the fluorescence intensity as shown in Fig. 11b and Table 4. The results show that as the concentration of tyrosine increased, the intensity of the fluorescence peak at 304 nm also increased correspondingly. In addition, under the same tyrosine concentration, the fluorescence intensity of the  $\text{ZnFe}_2\text{O}_4@\text{SiO}_2$ -NALC system with *L*-Tyr is always higher than that of the  $\text{ZnFe}_2\text{O}_4@\text{SiO}_2$ -NALC system with *D*-Tyr. These experimental results show that chiral  $\text{ZnFe}_2\text{O}_4@\text{SiO}_2$ -NALC nanoparticles can identify tyrosine enantiomers by fluorescence spectroscopy in solution. There was a linear relationship between the maximum emission intensity at 304 nm in the fluorescence spectrum and the concentration of tyrosine enantiomer (0.025~0.200  $\text{mmol} \cdot \text{L}^{-1}$ ), and the lowest detection limit of tyrosine was 25  $\mu\text{mol} \cdot \text{L}^{-1}$ .

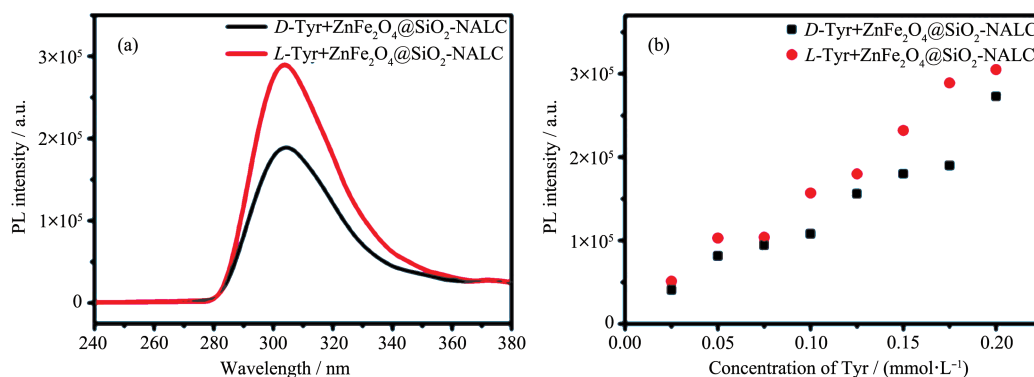


Fig. 11 (a) Fluorescence emission spectra ( $\lambda_{\text{ex}}=229$  nm) of  $\text{ZnFe}_2\text{O}_4@\text{SiO}_2$ -NALC in the presence of *L*-Tyr and *D*-Tyr (0.175  $\text{mmol} \cdot \text{L}^{-1}$ ); (b) Effect of Tyr concentration on fluorescence intensity of  $\text{ZnFe}_2\text{O}_4@\text{SiO}_2$ -NALC-Tyr system at  $\lambda_{\text{em}}=304$  nm

**Table 4** Fluorescence intensity ( $\lambda_{em}=304\text{ nm}$ ) of ZnFe<sub>2</sub>O<sub>4</sub>@SiO<sub>2</sub>-NALC in the presence of *D*-Tyr or *L*-Tyr with different concentrations

$c_{Tyr} /$ (mmol·L <sup>-1</sup> )	Fluorescence intensity of ZnFe <sub>2</sub> O <sub>4</sub> @SiO <sub>2</sub> -NALC	
	<i>L</i> -Tyr	<i>D</i> -Tyr
0.025	40 600	51 100
0.050	81 400	103 000
0.075	94 400	104 000
0.100	108 000	157 000
0.125	156 000	180 000
0.150	156 001	232 000
0.175	156 002	289 000
0.200	156 003	305 000

As shown in Fig.S6~S7 and Table S16~S19, the influence of pH value on the identification properties is discussed (using B-R buffer to adjust the pH value of the solution, the pH range was 2.22~9.18). The experimental phenomena show that under acidic or alkaline conditions, the fluorescence intensity showed that the maximum fluorescence intensity of *D*-Tyr was not always weaker than *L*-Tyr. The results indicate that ZnFe<sub>2</sub>O<sub>4</sub>@SiO<sub>2</sub>-NALC chiral nanomaterial is impossible to identify Tyr under acidic and alkaline conditions by fluorescence spectroscopy, only materials in a neutral environment can recognize Tyr enantiomers.

### 2.3 Chiral sensing mechanism

To explore and clarify the mechanism of chiral recognition is the key issue. Under the suitable experimental conditions, the selectivity between chiral substances is due to the preferential interaction between the chiral modifier and one of the enantiomers. In this experiment NALC and Tyr readily combine to construct diastereomers, with stability determined by the chirality of identified amino acids (*i. e.*, chirality of Tyr). And the same type of enantiomer to combine has a more stable structure because the stability of complexes depends on the steric hindrance and trans effect of the ligand<sup>[36-38]</sup>. Therefore, the ZnFe<sub>2</sub>O<sub>4</sub>@SiO<sub>2</sub>-NALC material has a stronger binding affinity with the *L*-Tyr than with the *D*-Tyr, thus achieving the purpose of chiral recognition.

### 3 Conclusions

In this study, we assemble a novel chiral nanoma-

terial ZnFe<sub>2</sub>O<sub>4</sub>@SiO<sub>2</sub>-NALC for enantioselective recognition of Tyr enantiomers. The assay described in this work is easily readout with using a UV-Vis spectra and fluorescence spectra. In comparison with common chiral recognition methods, the method is more attractive because of its cheapness and ready availability. This is the first application of the ZnFe<sub>2</sub>O<sub>4</sub>@SiO<sub>2</sub>-NALC for chiral recognition, opening up a new method for designing more effective enantioselective strategies. Furthermore, this work provides a cheap and convenient method for identifying other chiral enantiomers or compounds.

Supporting information is available at <http://www.wjhxxb.cn>

### References:

- [1] Zhang L, Xu C L, Liu C W, et al. *Anal. Chim. Acta*, **2014**,**809**: 123-127
- [2] Ghosh S, Fang T H, Uddin M S, et al. *Colloids Surf. B*, **2013**, **105**:267-277
- [3] Su H Y, Zheng Q L, Li H B. *J. Mater. Chem.*, **2012**,**22**:6546-6548
- [4] Sun Y, Zhang L, Li H B. *New J. Chem.*, **2012**,**36**:1442-1444
- [5] Jafari M, Tashkhourian J, Absalan G. *Talanta*, **2018**,**178**:870-878
- [6] Lomeli-Rosales D A, Rangel S, Zamudio-Ojeda A, et al. *ACS Omega*, **2016**,**1**:876-885
- [7] Song G X, Xu C L, Li B X. *Sens. Actuators B*, **2015**,**215**:504-509
- [8] Song G X, Zhou F L, Xu C L, et al. *Analyst*, **2016**,**141**:1257-1265
- [9] Wang Y, Zhou X, Xu C, et al. *Sci. Rep.*, **2018**,**8**:5296-5304
- [10] Zhang L, Xu C L, Song G X, et al. *RSC Adv.*, **2015**,**5**:27003-27008
- [11] Zor E. *Talanta*, **2018**,**184**:149-155
- [12] Carrillocarrión C, Cárdenas S, Simonet B M, et al. *Anal. Chem.*, **2009**,**81**:4730
- [13] Copur F, Bekar N, Zor E, et al. *Sens. Actuators B*, **2019**,**279**: 305-312
- [14] Delgado-Perez T, Bouchet L M, de la Guardia M, et al. *Chem. Eur. J.*, **2013**,**19**:11068-11076
- [15] Guo Y, Zeng X P, Yuan H Y, et al. *Spectrochim. Acta Part A*, **2017**,**183**:23-29
- [16] Yang J D, Tan X P, Zhang X N, et al. *Spectrochim. Acta Part A*, **2015**,**151**:591-597

- [17]Deng X J, Li W B, Ding G S, et al. *Sep. Purif. Rev.*, **2017**,**48**: 14-29
- [18]Yoo P S, Reddy D A, Jia Y, et al. *J. Colloid Interface Sci.*, **2017**,**486**:136-143
- [19]ZHAO Da-Lei(赵大雷), YANG Qun(杨群), LI Guang(李广). *Journal of Anhui University: Natural Science Edition*(安徽大学学报:自然科学版), **2017**,**41**:78-84
- [20]Chen S K, Sun Y, Li X, et al. *J. Solid State Chem.*, **2019**,**280**: 120994-121003
- [21]YU Min-Na(于敏娜), WEI Chang-Ping(魏长平), LIU Ying(刘颖). *Chemical Industry and Engineering Progress*(化工进展), **2010**,**29**:278-281
- [22]Ren C R, Ding X G, Fu H Q, et al. *RSC Adv.*, **2017**,**7**:6911-6921
- [23]Atia A A, Donia A M, Al-Amrani W A. *Chem. Eng. J.*, **2009**, **150**:55-62
- [24]Chang Q, Zhu L H, Yu C, et al. *J. Lumin.*, **2008**,**128**:1890-1895
- [25]Lan S, Wu X M, Li L L, et al. *Colloids Surf. A*, **2013**,**425**:42-50
- [26]Wang Q, Gao W, Liu Y, et al. *Chem. Eng. J.*, **2014**,**250**:55-65
- [27]Zhao W, Liang C, Wang B B, et al. *ACS Appl. Mater. Interfaces*, **2017**,**9**:41927-41936
- [28]Gao F, Ma S Y, Xiao X C, et al. *Talanta*, **2017**,**163**:102-110
- [29]Rabbani M, Heidari-Golafzani M, Rahimi R. *Mater. Chem. Phys.*, **2016**,**179**:35-41
- [30]Bieri M, Gautier C, Burgi T. *Phys. Chem. Chem. Phys.*, **2007**, **9**:671-685
- [31]Gautier C, Burgi T. *Chem. Commun.*, **2005**,**43**:5393-5395
- [32]Tashkhourian J, Afsharinejad M. *Anal. Methods*, **2016**, **8**: 2251-2258
- [33]Li S X, Liang W J, Zheng F Y, et al. *Sens. Actuators B*, **2016**, **224**:48-54
- [34]Rhim J W, Hong S I, Park H M, et al. *J. Agric. Food Chem.*, **2006**,**54**(16):5814-5822
- [35]Contino A, Maccarrone G, Zimbone M, et al. *J. Colloid Interface Sci.*, **2015**,**443**:30-35
- [36]Chen Z, Yamada K, Niitsuma M, et al. *Anal. Chim. Acta*, **2000**,**403**(1):173-178
- [37]Sabolović J, Tautermann C S, Loerting T, et al. *Inorg. Chem.*, **2003**,**42**:2268-2279
- [38]Hyeokseo S, Sudeok K, Suhan M. *Anal. Methods*, **2013**,**6**(1): 73-76